Exciton/Charge-transfer Electronic Couplings in Organic Semiconductors

Seth Difley and Troy Van Voorhis[*]

Department of Chemistry, Massachusetts Institute of Technology, Cambridge, MA 02139-4307

USA

E-mail: tvan@mit.edu

Abstract

Charge transfer (CT) states and excitons are important in energy conversion processes that occur in organic light emitting devices (OLEDS) and organic solar cells. An *ab initio* density functional theory (DFT) method for obtaining CT-exciton electronic couplings between CT states and excitons is presented. This method is applied to two organic heterodimers to obtain their CT-exciton coupling and adiabatic energy surfaces near their CT-exciton diabatic surface crossings. The results show the new method provides a new window into the role of CT states in exciton-exciton transitions within organic semiconductors.

Introduction

Organic semiconductors (OSCs) hold promise as low-cost solar cells[1–8] and as versatile, flexible, high-contrast display technologies[9–13] that are amenable to cost-effective large-scale production. Several of the challenges to improving the energy conversion efficiencies of these devices include

---

[*]To whom correspondence should be addressed

maximizing absorption (or emission) efficiencies, electron and hole transport, and charge collection (or charge recombination).[14,15] A detailed understanding of how these device properties are related to OSC materials and device architecture is important for guiding the design of semiconductor technologies. In this present study, we look closely at electronic couplings, which play an valuable role in providing this understanding.
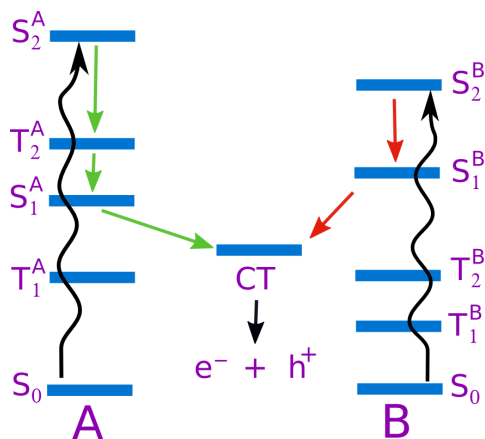

Figure 1: Two electron transfer pathways in an organic photovoltaic material. The spatial location (molecule A or B) of the localized excitons is denoted by superscript. The CT state is spread over both molecules.

One reason we might be interested in these couplings is that spatially localized excitons and long-range CT states play crucial roles in OSCs. Fig. Figure 1 illustrates the interplay of these states at a generic PV interface between OSC materials A and B. The first several localized singlet and triplet excitons are presented for each PV material. A nonlocal CT state that involves both A and B is also shown. Fig. Figure 1 shows two electronic state pathways that may be involved in free carrier generation. In the first step of the solar cell's operation cycle, the A-B system is photoexcited to a singlet excitonic state localized on either A or B. After some time, the system can undergo a series of relaxations from one exitonic state to another exitonic state and eventually relax to the CT state. Finally, the CT state can undergo charge separation to form free electron and hole charge carriers.[16] These charge carriers can drift toward the electrodes to produce the desired current. The overall rate of carrier generation depends on the rate of each step. In optimizing these devices, we wish to choose materials and device morphologies that maximize the rate of desirable

relaxation mechanisms while minimizing loss mechanism rates.[14] A useful tool for estimating electronic transition rates between states a and b is the Marcus rate expression

$$k_{ab} = \frac{2\pi}{\hbar}|H_{ab}|^2 \frac{1}{\sqrt{4\pi\lambda k_B T}} exp\left(\frac{-(\lambda + \Delta G^o)^2}{4\lambda k_B T}\right). \tag{1}$$

Here, ΔG^o is the driving force, λ is the reorganization energy and $H_{ab} = \langle\psi_a|H|\psi_b\rangle$ is the coupling between states described by the wave functions ψ_a and ψ_b and Hamiltonian H. Importantly, we note that the rate is proportional to the square modulus of the coupling. In this way, the coupling governs the relative magnitude of transition rates between states with similar driving forces and reorganization energies.

Another reason couplings are important is for the conceptual study of OSC electronic transition mechanisms. To begin this discussion, it is convenient to describe electronic energy surfaces as either being diabatic or adiabatic. Given non-orthogonal diabatic states with energies H_{aa} and H_{bb} and the coupling between these states H_{ab}, a generalized eigenvalue problem (Eq. 2) can be solved to obtain the corresponding adiabatic states $\psi^\pm \equiv d_a^\pm \psi_a + d_b^\pm \psi_b$ and energy surfaces $\varepsilon^\pm$

$$\begin{pmatrix} H_{aa} & H_{ab} \\ H_{ba} & H_{bb} \end{pmatrix} \begin{pmatrix} d_a^\pm \\ d_b^\pm \end{pmatrix} = \varepsilon_{ad}^\pm \begin{pmatrix} S_{aa} & S_{ab} \\ S_{ba} & S_{bb} \end{pmatrix} \begin{pmatrix} d_a^\pm \\ d_b^\pm \end{pmatrix} \tag{2}$$

An important distinction between diabatic and adiabatic states is that diabatic states are characterized by uniform electronic character as one moves along an arbitrary nuclear coordinate. Thus, if a state has ionic (covalent) character at one point on its diabatic surface, it will have ionic (covalent) character at every point on that diabatic surface. In contrast, adiabatic states, which result from rigorously applying the Born-Oppenheimer approximation, may have varied electronic character at different points on the same adiabatic energy surface. Another way to conceptualize the difference between diabatic and adiabatic states is that diabatic surfaces can energetically cross each other, while adiabatic surfaces instead undergo an "avoided crossing" near the diabatic crossings (Fig. Figure 2).
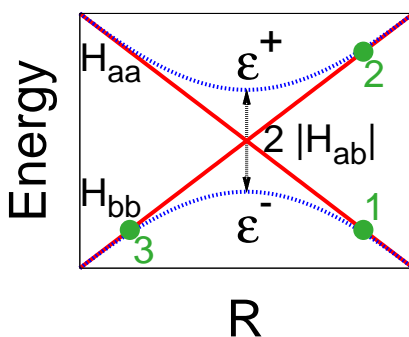
Figure 2: Cartoon of adiabatic (dashed curves labeled H_{aa} and H_{bb}) and diabatic states (solid curves labeled $\varepsilon^{\pm}$) at the crossing of the diabatic states as a function of some nuclear coordinate R. The coupling H_{ab} is half of the separation between the adiabatic states at the crossing. Points 1 and 3 are connected by an adiabatic state, while points 2 and 3 are connected by a diabatic state.

The interplay between diabatic and adiabatic states is important for understanding electronic transitions.[17] That is, neither diabatic nor adiabatic states can alone describe all mechanisms. For example, suppose in Fig. Figure 2 that the system has been excited onto the upper adiabatic energy surface at point 2. By following the diabatic state, the system relaxes to the lower adiabatic surface at point 3. Meanwhile, starting from point 1, the system must follow the adiabat to get to the "product" at point 3. To put it another way, in Fig. Figure 2 the system behaves diabatically when optically activated and adiabatically when thermally activated. The relative magnitude of these rates is governed by the electronic coupling, making it is an important quantity for the mechanistic description of OSCs.

In this study, we present an *ab initio* method for obtaining electronic couplings in which the CT states are generated by constrained DFT (CDFT)[18] and the excitons are generated by time dependent density functional theory (TDDFT).[19] This effort represents an expansion of previous work that described a method for obtaining electronic couplings between pairs of CDFT states.[20] In addition to being *ab initio*, the approach described in this study takes advantage of the balance between accuracy and computational tractability that the TDDFT and CDFT methods offer for excited states. After having demonstrated the method's utility for constructing the adiabatic states of two specific and relevant organic dimers, we will briefly discuss implications of our coupling

4

results for OSC electron and hole transport.

Methods

Linear response TDDFT

Linear response time independent density function theory (TDDFT) is a successful method for obtaining excited state properties based solely on the response of the electron density.[19] The central object in linear response is the transition density for the i→f excitation,

$$\rho_{i \to f}(r) = \langle \Psi_i | \delta(\hat{r} - r) | \Psi_f \rangle. \tag{3}$$

Together with the transition energy, $\omega_{i \to f}$, $\rho_{i \to j}$ contains all the information needed to determine the intensity of the transition under an arbitrary field. In TDDFT, the transition density is expanded in terms of products of the occupied (ϕ_j) and unoccupied (ϕ_b) Kohn Sham (KS) orbitals as:[21]

$$\rho_{i \to f}(r) = \sum_{jb} \left(X_{jb} \phi_b(r) \phi_j^*(r) + Y_{jb} \phi_j(r) \phi_b^*(r) \right). \tag{4}$$

The X and Y amplitudes that appear in this expansion can be thought of, roughly, as the amplitudes for $j \to b$ excitation and $b \to j$ de-excitation in the given transition. These amplitudes are easily calculated using any of a number of existing implementations of the linear response TDDFT equations.

While KS-TDDFT relies on a single determinant ansatz for the ground state and only explicitly considers single excitation/de-excitation terms in computing the response, yet it can be proven that TDDFT gives the **e**xact $\omega_{i \to f}$ and $\rho_{i \to j}$ if the exact exchange-correlation kernel, f_{xc} is used.[22] Unfortunately, the exact kernel is unknown, so one resorts to one of various approximations in order to apply TDDFT to molecules. For example, one commonly assumes that f_{xc} is frequency independent (the adiabatic approximation) and/or local in space (local density approximation). One

common weakness of the vast majority of these commonly used functionals is that they do not treat charge transfer excitations on the same footing with localized valence excitations.[23] Typically, the CT states are far too low in energy - by an eV or more in some cases - leading to very poor energy landscapes.[24] In practice, this problem can be softened by the use of range-separated hybrid functionals.[25,26] By design, these functionals treat long-range CT excitations correctly, but this comes at the expense of also systematically raising valence excitation energies.[27] Within our group, we have explored the alternative possibility of treating CT states with constrained DFT (as described below) and using TDDFT for only the valence exciton states.

Before moving on to discuss constrained DFT, we make one note about how we will use TDDFT. In order to compute the coupling, we will need a surrogate wave function, Φ^{ex}, for the TDDFT exciton. A simple ansatz for Φ^{ex} forces the transition density between Φ^{ex} and the KS determinant to be equal to the TDDFT transition density:

$$\langle \Phi_0 | \delta(\hat{r} - r) | \Phi^{ex} \rangle \equiv \rho_{i \to f}(r) = \sum_{jb} \left(X_{jb} \phi_b(r) \phi_j^*(r) + Y_{jb} \phi_j(r) \phi_b^*(r) \right). \tag{5}$$

This serves as an implicit definition of Φ^{ex}. We note that this *will not* give us the exact excited state wave function any more than the Kohn-Sham determinant gives us the exact ground state wave function. Rather, this prescription gives us an approximate wave function that preserves an important physical property of the true system: the transition density. If we restrict our attention to single excitations from the KS reference, it is easily verified that

$$|\Phi^{ex}\rangle = \sum_{jb} (X_{jb} + Y_{jb}) |\Phi_j^b\rangle \equiv \sum_{jb} C_{jb} |\Phi_j^b\rangle \tag{6}$$

where Φ_j^b denotes the KS single determinant where the jth occupied orbital has been replaced by the bth unoccupied orbital. Similar manipulations have been performed previously in order to associate a wave function with a TDDFT transition.[28]

For the exact density functional, TDDFT states are rigorously adiabatic states because they obey the Born-Oppenheimer approximation. However, for commonly used approximate function-

als, we typically observe that the TDDFT states behave as diabatic or diabatic-like states. Although there are TDDFT states that involve a single molecule (e.g. a Frenkel exciton) and states that involve more than one molecule (e.g. CT between a pair), these two types of states are generally energetically well separated, which essentially ensures they will behave diabatically. Identifying the character of a given TDDFT state can be done by attachment/detachment density analysis.[29,30] If the attachment density is confined to the same molecule as the detachment density, the state is identified as an exciton. On the other hand, if the attachment density for a TDDFT state is on a different molecule than the detachment density, the TDDFT state is identified as a CT state. This attachment/detachment analysis can be conducted at several points along a given TDDFT surface to confirm that the electronic character remains consistent from one location on the surface to another. We also note that since excitons are localized on single monomers (i.e. they are Frenkel-type excitons), exciton energies obtained for dimer systems at large monomer-monomer separations are expected to be essentially the same as exciton energies obtained for a single monomer. Therefore, dimer TDDFT energies that do not connect to a sum of monomer TDDFT energies at large separation are typically identified as CT states.

Constrained DFT for diabatic states

Constrained density functional theory (CDFT) has been shown to be a reliable, inexpensive method for obtaining long-range CT state energies. The details of this approach have been presented elsewhere. [18,20,31–33] Here, we briefly review CDFT and illustrate the use of this computational tool as it pertains to obtaining electronic couplings.

In the CDFT formalism, we build constraints of the form

$$\sum_{\sigma} \int w_c^{\sigma}(\mathbf{r}) \rho^{\sigma}(\mathbf{r}) d\mathbf{r} = N_c \tag{7}$$

where the sum is over spins such that $\sigma = \alpha$ or β, c is the constrained region of the system, w_c is a weighting function that corresponds to the constrained property and N_c is the expectation value

of the constrained property. Eq. 7 is then combined as a Lagrange multiplier constraint with the Kohn-Sham energy functional $E[\rho]$ to generate a new functional

$$W[\rho, \{V_c\}] = E[\rho] + \sum_c^m V_c \left(\sum_\sigma \int w_c^\sigma(\mathbf{r}) \rho^\sigma(\mathbf{r}) \, d\mathbf{r} - N_c \right), \tag{8}$$

where the cth Lagrange multiplier is V_c, and there are m constraints. W is then made stationary with respect to ρ and V_c. By this procedure, we obtain the energy $E(\rho)$ as a natural function of the expectation value N_c. In the present study of electronic couplings, spin polarized CT states are generated by applying both charge and spin constraints via Eq. 7. A charge constraint is applied that forces the donor (acceptor) molecule to have an excess charge of $+1$ (-1). A concurrent constraint on the net spin forces the donor and acceptor, respectively, to have excess spin of $\pm\frac{1}{2}$. Importantly for the present study, applying these constraints produces CT states that are rigorously diabatic.

Electronic couplings between TDDFT and CDFT states

The electronic couplings whose properties are the focus of this study are

$$H_{ab} = \langle \psi^{CT} | H | \psi^{ex} \rangle, \tag{9}$$

where ψ_{CT} and ψ_{ex} are the wave functions corresponding to the CT state and exciton and H is the electronic Hamiltonian. In particular, we are interested in computing the electronic coupling between CT states obtained by CDFT and excitons obtained by TDDFT. To do this, we adapt the constrained approach that has been successfully demonstrated for obtaining couplings between CT and neutral states.[20]

In the constrained approach to electronic couplings, we use Kohn-Sham determinants to approximate the true wave function. This allows us to write the coupling matrix element (Eq. 9) in

terms of a single electronic density. Following this approach, we obtain[20]

$$H_{ab} = (E_{CT} + V_c^{CT} N_c)\langle \Phi^{CT}|\Phi^{ex}\rangle - V_c^{CT}\langle \Phi^{CT}|w_c|\Phi^{ex}\rangle. \tag{10}$$

Here, E_{CT} is the energy of $|\Phi^{CT}\rangle$, $\langle \Phi^{CT}|\Phi^{ex}\rangle$ is the CT-exciton overlap, V_c^{CT} is the CT state's constraining potential (Eq. 8), and $\langle \Phi^{CT}|w_c|\Phi^{ex}\rangle$ is the CT-exciton matrix element of the one-body weight operator w_c. This result makes the reasonable assertion that the electronic coupling depends on both the magnitude of the orbital overlap and the strength of the potential that was used to create the CT state.

For the true density functional, $\langle \Phi^{CT}|H|\Phi^{ex}\rangle$ is the complex conjugate of $\langle \Phi^{ex}|H|\Phi^{CT}\rangle$. However, applying the same logic as above we find $H_{ba} = \langle \Phi^{ex}|H|\Phi^{CT}\rangle = E_{ex}\langle \Phi^{ex}|\Phi^{CT}\rangle - V_c^{ex}\langle \Phi^{ex}|w_c|\Phi^{CT}\rangle$, where V_c^{ex} is the constraining potential corresponding to the exciton. For the approximate functionals that are commonly used, these two expressions are not equivalent, so the Hermiticity condition is not fulfilled. To satisfy Hermiticity, we choose the electronic coupling to be the average of H_{ab} and H_{ba}. This average is reasonable because H_{ab} overestimates the electronic coupling when H_{ba} underestimates the coupling, and vice versa.

Eq. 10 reduces the problem of computing the coupling to obtaining a zero-body overlap and one-body weight matrix element. In order to obtain a reasonable approximation to these matrix elements for excion-CT coupling, we note that both CDFT and TDDFT states can be expressed in terms of Slater determinants. Therefore, the coupling in Eq. 10 can be computed as a sum of zero- and one-body matrix elements of Slater determinants (Eqs. 11 and 12).[34]

$$\langle \Phi^{CT}|\Phi^{ex}\rangle = \sum_{ia}\langle \Phi^{CT}|\Phi^{ex}_{ia}\rangle C_{ia} \tag{11}$$

$$\langle \Phi^{CT}|w_c|\Phi^{ex}\rangle = \sum_{ia}\langle \Phi^{CT}|w_c|\Phi^{ex}_{ia}\rangle C_{ia} \tag{12}$$

In these equations, we have used the fact that the aproximate TDDFT states can written as sums of Slater determinants (Eq. 6). Computing each $\langle \Phi^{CT}|\Phi^{ex}_{ia}\rangle$ and $\langle \Phi^{CT}|H|\Phi^{ex}_{ia}\rangle$ term has an N^3

computational complexity, where N is the number of electrons in the system.[34] Furthermore the sums in Eqs. 11 and 12 are over occupied and virtual orbitals, both of which scale with the number of electrons in the system. Therefore, the total complexity of computing $\langle \Phi^{CT} | \Phi^{ex} \rangle$ or $\langle \Phi^{CT} | H | \Phi^{ex} \rangle$ is of order $N^3 \times N^2 = N^5$. With this complexity scaling, computing the coupling of even medium-sized molecular systems becomes intractable.

To decrease the complexity scaling of the coupling calculation, we use a Thouless rotation[35] to re-express the TDDFT excited states (Eq. 6) as a sum of two Slater determinants. In particular, we define $\phi_i(\pm\varepsilon) \equiv \phi_i \pm \varepsilon \sum_a C_i^a \phi_a$ where ε is small, ϕ_i is the ith occupied Kohn-Sham orbital and ϕ_a is the ath virtual Kohn-Sham orbital. That is, we construct new orbitals $\phi_i(\pm\varepsilon)$ that mix small amounts of the virtual orbitals with each the ith occupied orbitals. From these constructed orbitals, we build a pair of Slater determinants $\Phi(\pm\varepsilon) \equiv |\phi_1(\pm\varepsilon)\phi_2(\pm\varepsilon)\phi_3(\pm\varepsilon)\ldots| = |\phi_1\phi_2\phi_3\ldots| \pm \varepsilon \sum_{ia} C_i^a \phi_i^a + O(\varepsilon^2)$. Using these definitions, the TDDFT state becomes

$$|\Phi^{ex}\rangle = \sum_{ia} C_i^a \Phi_i^a = \lim_{\varepsilon \to 0} \left(\frac{\Phi(+\varepsilon) - \Phi(-\varepsilon)}{2\varepsilon} \right) \tag{13}$$

With the TDDFT state expressed in this two determinant form, the matrix element of Eq. 11 has the manageable computational complexity of $O(N^3)$.

TDDFT states $|\Phi^{ex}\rangle$ are generally not orthogonal to the CDFT states $|\Phi^{CT}\rangle$ because the two states eigenstates of different Hamiltonians. For this reason, we apply an orthogonalization step to put the couplings we obtain here on the same footing as couplings obtained by other methods. We define $S_{ij} = \langle \Psi^i | S | \Psi^j \rangle$ and weight matrix $w_c^{ij} = \langle \Psi^i | w_c | \Psi^j \rangle$, and solve for the generalized eigenstates of the constraint function

$$\begin{pmatrix} w_c^{aa} & w_c^{ab} \\ w_c^{ba} & w_c^{bb} \end{pmatrix} \begin{pmatrix} x_a^n \\ x_b^n \end{pmatrix} = n \begin{pmatrix} S_{aa} & S_{ab} \\ S_{ba} & S_{bb} \end{pmatrix} \begin{pmatrix} x_a^n \\ x_b^n \end{pmatrix}$$

where $\mathbf{x}^n$ is an eigenvector of $\mathbf{w_c}$ and n is its eigenvalue. By construction, the eigenstates of w_c are orthonormal and localized. We therefore transform the Hamiltonian to the eigenbasis of w_c via

$\mathbf{\tilde{H} = X^\dagger H X}$ and the appropriate (orthogonal) coupling is then given by the off-diagonal element $\tilde{H}_{ab}$.

A variety of methods have been developed for obtaining electronic couplings. In particular, if adiabatic energy surfaces are available, the coupling at the avoided crossing can be identified as one-half of the minimum energy separation between the adiabatic surfaces (Fig. Figure 2).[36] For obtaining couplings away from the avoided crossing, Mulliken-Hush methods[37] are often applied. A number of other empirical and semi-empirical approaches for obtaining couplings between various types of electronic states have also been developed.[38-43] The present approach is specialized in that it predicts couplings between two classes of states for which adiabatic energies are not easily obtained.

Computational Details

In this paper, we use the 3-21G basis set, B3LYP hybrid density functional, DFT, CDFT, and full linear response TDDFT as implemented in Q-Chem.[44] The basis set is intentionally small to speed up the calculations. Since this is a validation study and our conclusions are largely qualitative we do not anticipate that a larger basis would change the picture significantly. Becke weights[45] are used in the constrained population analysis. Attachment/detachment analysis[29] is used to obtain the electronic spatial character of the TDDFT states.

Diabatic energy surfaces for the chosen dimers are produced by making the monomer planes parallel, scanning along the separation distance between the monomer planes, and obtaining TDDFT and CDFT states for each separation distance. For the heterodimers studied, the CDFT constraints were chosen to obtain the lowest energy CT state.

Results

Triphenylene:1,3,5-trinitrobenzene

As a first illustration of the TDDFT/CDFT coupling method, we chose a dimer consisting of triphenylene (1,3,5-trinitrobenzene) as the donor (acceptor). The small size of these molecules allows a straightforward search for CT-exciton intersections and demonstrates many of the issues that arise in obtaining the electronic couplings of long-range organic dimers.
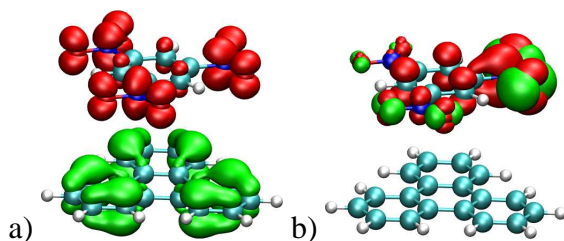

Figure 3: Attachment/detachment density plots for triphenylene:1,3,5-trinitrobenzene illustrating a) nonlocal CT-like and b) localized exciton-like electron densities. Red (green) regions have excess (deficient) density compared to the ground state.

The attachment/detachment density plots in Fig. Figure 3 show the qualitative difference between exciton and long-range CT-like states obtained by TDDFT for triphenylene:1,3,5-trinitrobenzene. In the analysis that follows, we will focus our attention on the TDDFT states that are manifested by localized densities such as in Fig. Figure 3b.

Fig. Figure 4 presents the first several singlet TDDFT states and the lowest lying CDFT state of triphenylene:1,3,5-trinitrobenzene. By attachment/detachment analysis, we find that the lowest nine states have CT-like electronic character as in the left pane of Fig. Figure 3, while the higher lying TDDFT states shown in Fig. Figure 4 have localized excitonic electronic character (Fig. Figure 3b). It is known that for many density functionals such as B3LYP, CT-like states generated by TDDFT have erroneously low energies.[24] Consequently, the lowest nine TDDFT states (red curves) in Fig. Figure 4 do not correspond to experimentally observable excitations and we will thus attempt to disregard these states in what follows. Meanwhile, the higher-lying singlet excitations represented by the green curves in Fig. Figure 4 are excitons and are expected to correspond
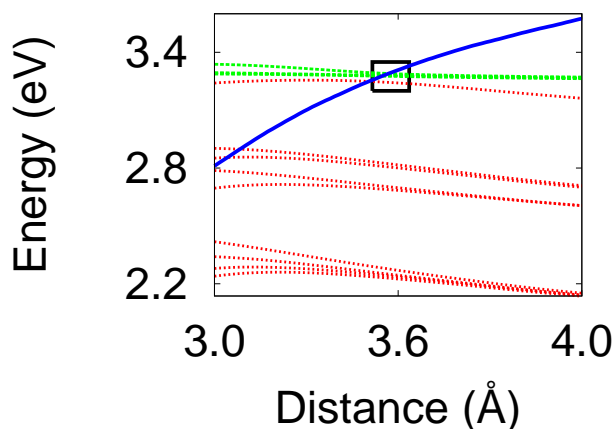
12

Figure 4: Diabatic energy surfaces for TDDFT excitons (dashed green curves), TDDFT CT-like states (dotted red curves) and a CDFT CT state (solid blue curve) for triphenylene:1,3,5-trinitrobenzene as a function of monomer-monomer separation distance. The inset rectangle encloses crossings of the CT state with three TDDFT excitons and one CT-like TDDFT state.

to fluorescence absorption spectra and form the exciton states of interest.

Excitons are localized on monomers, so they should not change much in energy as the monomer-monomer separation increases. This expectation that exciton energies will remain nearly constant with respect to separation distance provides a diagnostic for distinguishing excitons from TDDFT CT-like states that compliments attachment/detachment analysis. For this particular dimer, we find that the exciton TDDFT states in Fig. Figure 4 remain at nearly constant energies with respect to the separation distance, but that the CT-like states erroneously *decrease* in energy as the monomer-monomer separation distance is increased. Meanwhile, CT states are characterized by charge separation between the two monomers. Thus, one would expect CT state energies to increase as the monomers are separated due to the attractive $\frac{1}{r}$ Coulombic potential between the CT state's separated charges. Indeed, we find that the CT state generated by CDFT has a positive slope over the entire range presented in Fig. Figure 4. This points out precisely why we use CDFT to obtain CT states and TDDFT to obtain excitons: CDFT correctly describes CT states, but knows nothing of the TDDFT excitons.

Since we will treat the TDDFT excitons as diabatic-like states, it is important that they have consistent electronic character as we track along the monomer-monomer separation coordinate.

We observe in Fig. Figure 4 that all but one of the CT-like TDDFT states are separated in energy from the excitons. Only the highest lying CT-like TDDFT state ever approaches the three lowest lying excitons S_1, S_2 and S_3, and even then only at separations less than 3.7 Å. The attachment/detachment densities of S_1, S_2 and S_3 were inspected near 3.5 Å. S_1 and S_2 were found to have localized densities in this monomer-monomer separation range. S_3 is also primarily localized over the entire range presented in Fig. Figure 4, only showing a small amount of charge separation near 3.5 Å,.
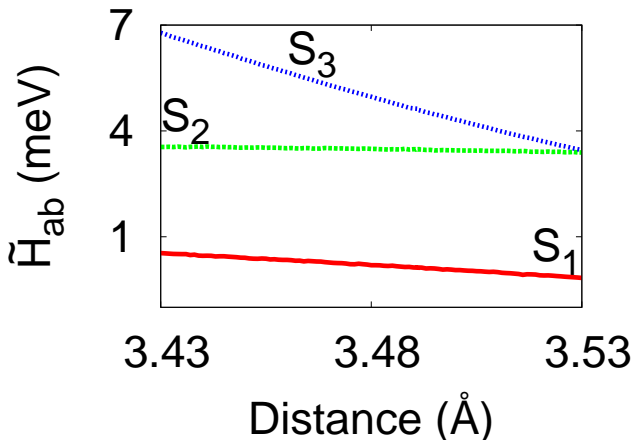

Figure 5: CT-exciton Coupling magnitudes $\tilde{H}_{ab}$ for triphenylene:1,3,5-trinitrobenzene at the diabatic state crossings in Fig. Figure 4 as a function of the monomer-monomer separation distance. Labels indicate which exciton is coupled to the CT state. We find that the couplings tend toward zero at large separations.

The triphenylene:1,3,5-trinitrobenzene CDFT state intersects three TDDFT states in the inset rectangle of Fig. Figure 4. We computed couplings $\tilde{H}_{ab}$ between the CT state and these three excitons in the region of the crossings. Fig. Figure 5 presents the resulting coupling magnitudes. We observe that the couplings are on the order of 1-7 meV and that $\tilde{H}_{CT,S_3} > \tilde{H}_{CT,S_2} > \tilde{H}_{CT,S_1}$. Therefore, if the reorganization energies and driving forces are similar, we expect transitions between S_3 and the CT state to occur more easily than transitions between S_2 or S_1 and the CT state (Eq. 1). Another observation is that the couplings tend toward zero for large monomer-monomer separations. This reflects the decreasing orbital overlap between the exciton and CT state. Additionally, we note that although the attachment/detachment density of S_3 shows mild charge separation near

3.5 Å, the magnitudes shown in Fig. Figure 5 are consistently small as would be expected for couplings between exciton-like TDDFT states and CT states. It is therefore reasonable to treat S_1, S_2, and S_3 as diabatic states.
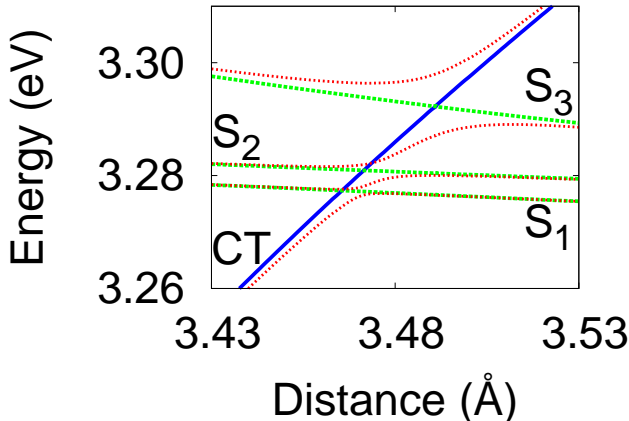

Figure 6: Diabatic exciton states (labeled green dashed curves), CT state (labeled solid blue curve), and adiabatic states (dotted red curves) of triphenylene:1,3,5-trinitrobenzene at the intersections of the CT state with S_1, S_2, and S_3.

The four adiabatic states that result from solving Eq. 2 for the CT, S_1, S_2, and S_3 diabatic states and couplings are shown in Fig. Figure 6. We observe that the adiabatic states avoid each where the diabatic states intersect. Also, the magnitude of the avoided crossing is directly related to the associated coupling magnitude. That is, the adiabatic states near the CT-S_1 (S_3) crossing most narrowly (strongly) avoid each other because the coupling between these states is small (large). Meanwhile, for regions on the energy surfaces far from avoided crossings, the adiabatic states are almost identical to the diabatic states. Importantly, Fig. Figure 6 provides a concrete pathway for a nonadiabatic transition in an organic heterodimer. For example, suppose that the triphenylene:1,3,5-trinitrobenzene dimer is initially excited to the highest-lying exciton in Fig. Figure 6 and consider how it might generate trapped charge carriers. In the diabatic picture, S_3 can transition to the CT state (at around 3.5 Å) and directly relax by dragging the two monomers closer together, trapping the electron and hole. Describing the same mechanism in the adiabatic picture would require starting in the 4th adiabat and making a rapid succession of nonadiabatic jumps ($4 \rightarrow 2 \rightarrow 3 \rightarrow 1$). This is not to say that this particular mechanism is operative in this particular dimer;

15

merely that a mechanism like this is much easier to describe with the diabatic coupling than with traditional adiabatic states. We note that a similar mechanism ($S_3 \rightarrow CT \rightarrow S_1$) could be used to describe nonradiative relaxation between different bright exciton states mediated by the dark CT state.

Zn-porphyrin:PTCBI

We have seen that the triphenylene:1,3,5-trinitrobenzene dimer provides an interesting technical demonstration of the constrained coupling method. Let us now study the CT-exciton couplings and resulting adiabatic states of a dimer composed of two organic dyes commonly used in organic semiconductors. PTCBI (3,4,9,10-perylenetetracarboxylic-bis-benzimidazole) is an organic dye often used as as an electron acceptor in OSCs.[1,46,47] It absorbs in the 450-800 nm range with absorption maxima near 525 and 700 nm.[48] Meanwhile, Zn-porphyrin is commonly used in dye-sensitized solar cells[49] and in porphyrin-fullerene solar cells.[50] Porphyrins have an absorption onset near 450 nm[51] and have an important role in photosynthetic systems.[52,53]
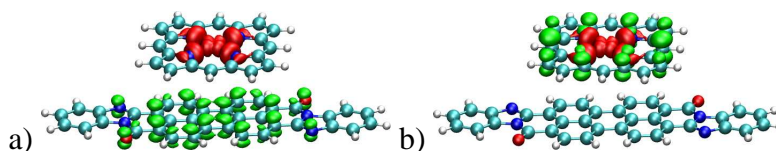

Figure 7: Attachment/detachment density plots for Zn-porphyrin:PTCBI illustrating a) nonlocal CT-like and b) localized exciton-like TDDFT states. Red (green) regions have excess (deficient) density compared to the ground state.

As for triphenylene:1,3,5-trinitrobenzene (Fig. Figure 3), we use attachment/detachment analysis to identify TDDFT states with excitonic character. Fig. Figure 7 contains representative CT-like and excitonic TDDFT densities.

Fig. Figure 8 presents the first several singlet TDDFT states and the lowest lying CDFT state of Zn-porphyrin:PTCBI. As for triphenylene:1,3,5-trinitrobenzene (Fig. Figure 4), we find that the CDFT state has a positive slope for the entire range inspected. By attachment/detachment analysis, the three TDDFT states below 1.7 eV are identified as CT-like. That is, the lowest singlet exciton
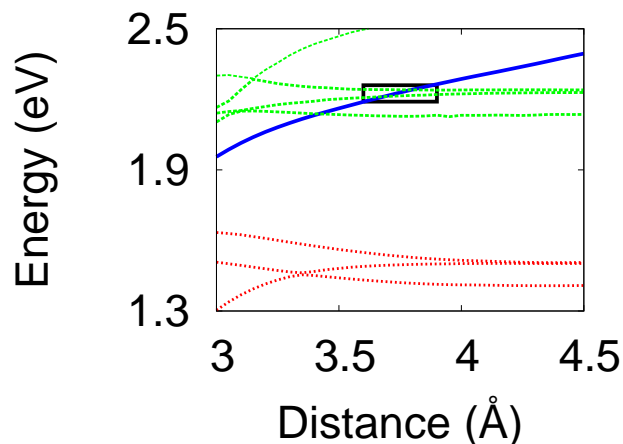
Figure 8: Diabatic energy surfaces for TDDFT excitons (dashed green curves), TDDFT CT-like states (dotted red curves) and a CDFT state (solid blue curve) for Zn-porphyrin:PTCBI as a function of monomer-monomer separation distance. The inset rectangle encloses crossings of the CT state with two TDDFT excitons. We see that the localized TDDFT states are energetically separated from the CT-like TDDFT states.

states appear above 2.1 eV. Unlike for triphenylene:1,3,5-trinitrobenzene, there is an energetic delineation between the CT-like TDDFT states and the excitons, leading to clearly diabatic-like states.
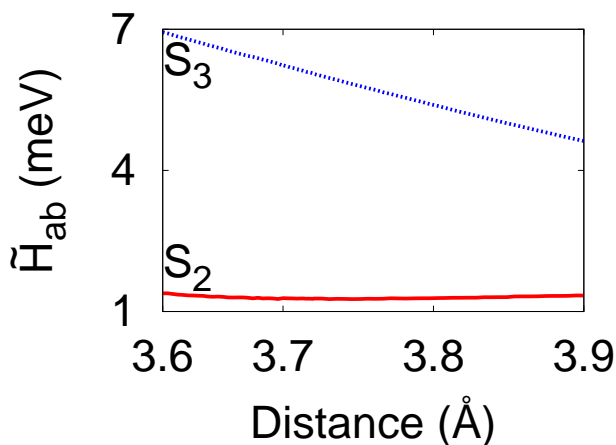

Figure 9: Coupling magnitudes near the CT-S_2 and CT-S_3 intersections labeled by the coupled exciton. We find that the CT-S_2 coupling is small over the entire range, and that the CT-S_3 couplings tends toward zero at large separations.

In Fig. Figure 8, the CT state intersects three TDDFT states. Fig. Figure 9 presents coupling magnitudes $\tilde{H}_{ab}$ for the upper two of these intersections. As in triphenylene:1,3,5-trinitrobenzene

17

(Fig. Figure 5), we observe that the couplings are on the order of 0-7 meV and tend toward zero for large monomer-monomer separations. We note that the CT-S_3 coupling is much larger than the CT-S_2 coupling. Thus, by Eq. 1, we might expect more facile transitions between S_3 and the CT state than between S_2 and the CT state.
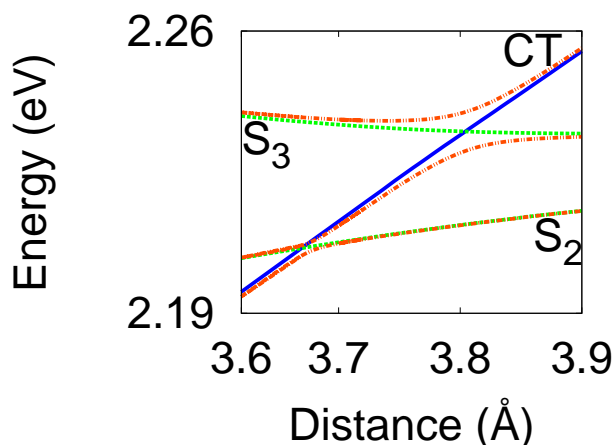

Figure 10: Diabatic exciton states (labeled green dashed curves), CT state (labeled solid blue curve), and adiabatic states (dotted red curves) of Zn-porphyrin:PTCBI at the intersections of the CT state with S_2 and S_3.

Fig. Figure 10 presents adiabatic and diabatic CT and exciton energy surfaces in the region of the CT-S_2 and CT-S_3 intersections. We observe that the adiabatic states avoid each where the diabatic states intersect. The the avoided crossing magnitudes correspond to their associated coupling magnitude so that the adiabatic states near the CT-S_2 (S_3) crossing narrowly (strongly) avoid each other. Meanwhile, for regions on the energy surfaces far from avoided crossings, the adiabatic states are almost identical to the diabatic states. As for triphenylene:1,3,5-trinitrobenzene, we see in Fig. Figure 10 that exciton relaxation in Zn-porphyrin:PTCBI can be mediated by CT states. Given the roles of PTCBI and Zn-porphyrin as commonly used semiconductor devices, these mechanistic details about their nonadiabatic transitions are of particular interest for guiding the design of advanced solar cells and light-emitting devices.
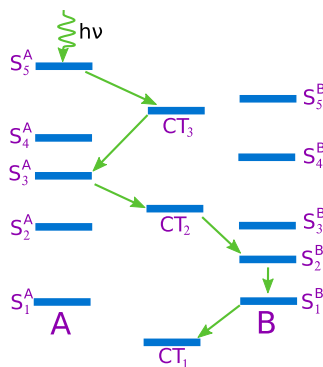
Figure 11: Illustration of CT-state mediated exciton-exciton transitions ($S_n \rightarrow CT \rightarrow S_{n-1}$).

Conclusions

We have presented an *ab initio* method for obtaining the electronic couplings between excitons and CT states in organic molecules. The utility of this method has been demonstrated by applying it to the study of the adiabatic and diabatic states and nonadiabatic transitions of two organic dimers. These results provide conceptual details of the mechanisms that allow transitions between CT states and excitons, which is an integral step in the efficient function of organic solar cells and light-emitting devices. In particular, these results show how CT states can play an important role in mediating exciton-exciton transitions (Fig. Figure 11) and conversion of excitons to free carriers.

These calculations show that it is possible to properly couple the lowest-lying CT state to a manifold of exciton states using CDFT and TDDFT in concert. Moving forward, one would like to extend this method in a number of ways. First, it would be nice if CT states other than the lowest CT state could be treated - this would allow us to characterize ultrafast relaxation involving higher-lying CT states. Second, there is a significant amount of user input that goes into these calculations - most notably the user must identify the Frenkel-like exciton states from TDDFT amidst a sea of spurious CT states. Ideally, this screening process would be automatic. For example, one could restrict the TDDFT calculation *a priori* to include only localized excitations. This would eliminate the need to screen the states manually and could potentially speed up the TDDFT calculations significantly. Finally, the calculations presented in this work have been conducted in the gas phase. Future efforts to compute these CT-exciton couplings will use condensed phase methods such as

QM/MM[54,55] and implicit solvation models[56] that simulate effects due to bulk polarization and nuclear heterogeneity. These bulk calculations provide reorganization energies and driving forces that may be combined with the electronic couplings to provide estimates of OSC transition rates.

Acknowledgement

References

(1) Tang, C. W. *Appl. Phys. Lett.* **1986**, *48*, 183–185.

(2) Li, G.; Shrotriya, V.; Huang, J. S.; Yao, Y.; Moriarty, T.; Emery, K.; Yang, Y. *Nat. Mater.* **2005**, *4*, 864–868.

(3) Xue, J.; Rand, B. P.; Uchida, S.; Forrest, S. R. *Adv. Mater.* **2005**, *17*, 66–70.

(4) Park, S. H.; Roy, A.; Beaupr, S.; Cho, S.; Coates, N.; Moon, J. S.; Moses, D.; Leclerc, M.; Lee, K.; Heeger, A. J. *Nat. Photonics* **2009**, *3*, 297–302.

(5) Kim, J. Y.; Lee, K.; Coates, N. E.; Moses, D.; Nguyen, T.; Dante, M.; Heeger, A. J. *Science* **2007**, *317*, 222–225.

(6) Koster, L. J. A.; Mihailetchi, V. D.; Blom, P. W. M. *Appl. Phys. Lett.* **2006**, *88*, 093511.

(7) Rand, B. P.; Burk, D. P.; Forrest, S. R. *Phys. Rev. B* **2007**, *75*, 115327.

(8) Riede, M.; Mueller, T.; Tress, W.; Schueppel, R.; Leo, K. *Nanotechnology* **2008**, *19*, 424001.

(9) Helfirch, W.; Scheinder, W. G. *Phys. Rev. Lett.* **1965**, *14*, 229–231.

(10) Pope, M.; Kallmann, H. P.; Magnante, P. *J. Chem. Phys.* **1963**, *38*, 2042–2043.

(11) van Slyke, S. A.; Tang, C. W. *Appl. Phys. Lett.* **1987**, *51*, 913–915.

(12) Burroughes, J. H.; Bradley, D. C. C.; Brown, A. R.; Marks, R. N.; Mackay, K.; Friend, R. H.; Burns, P. L.; Holmes, A. B. *Nature* **1990**, *347*, 539–541.

(13) Baldo, M. A.; Thompson, M. E.; Forrest, S. R. *Nature* **2000**, *403*, 750–753.

(14) Heremans, P.; Cheyns, D.; Rand, B. *Acc. Chem. Res.* **2009**, *42*, 1740–1747.

(15) Nelson, J.; Kwiatkowski, J. J.; Kirkpatrick, J.; Frost, J. M. *Acc. Chem. Res.* **2009**, *42*, 1768–1778.

(16) Zhu, X.-Y.; Yang, Q.; Muntwiler, M. *Acc. Chem. Res.* **2009**, *42*, 1779–1787.

(17) Brédas, J.-L.; Beljonne, D.; Coropceanu, V.; Cornil, J. *Chem. Rev.* **2004**, *104*, 4971–5004.

(18) Wu, Q.; Voorhis, T. V. *Phys. Rev. A* **2005**, *72*, 024502.

(19) Gross, E. K. U.; Dobson, J. F.; Petersilka, M. *Top. Curr. Chem.* **1996**, *181*, 81.

(20) Wu, Q.; Voorhis, T. V. *J. Chem. Phys.* **2006**, *125*, 164105.

(21) Furche, F. *J. Chem. Phys.* **2001**, *114*, 5982–5992.

(22) Runge, E.; Gross, E. K. U. *Phys. Rev. Lett.* **1984**, *52*, 997.

(23) Maitra, N. T. *J. Chem. Phys.* **2005**, *122*, 234104.

(24) Dreuw, A.; Head-Gordon, M. *J. Am. Chem. Soc.* **2004**, *126*, 4007–4016.

(25) Vydrov, O. A.; Scuseria, G. E. *J. Chem. Phys.* **2006**, *125*, 234109.

(26) Yanai, T.; Tew, D. P.; Handy, N. C. *Chemical Physics Letters* **2004**, *393*, 51–57.

(27) Jacquemin, D.; Perpète, E. A.; Scuseria, G. E.; Ciofini, I.; Adamo, C. *J. Chem. Theor. Comp.* **2008**, *4*, 123–135.

(28) Wong, C. Y.; Curutchet, C.; Tretiak, S.; Scholes, G. D. *J. Chem. Phys.* **2009**, *130*, 081104.

(29) Head-Gordon, M.; Graña, A. M.; Maurice, D.; White, C. A. *J. Chem. Phys.* **1995**, *99*, 14261–14270.

(30) Martin, R. L. *J. Chem. Phys.* **2002**, *118*, 4775–4777.

(31) Rudra, I.; Wu, Q.; Voorhis, T. V. *J. Chem. Phys.* **2006**, *124*, 24103.

(32) Wu, Q.; Voorhis, T. V. *J. Phys. Chem. A* **2006**, *110*, 9212–9218.

(33) Wu, Q.; Van Voorhis, T. *J. Chem. Theory Comput.* **2006**, *2*, 765–774.

(34) Löwdin, P.-O. *Phys. Rev.* **1955**, *97*, 1474–1489.

(35) Thouless, D. J. *Nuc. Phys.* **1960**, *21*, 225–232.

(36) Coropceanu, V.; Cornil, J.; da Silva Filho, D.; Olivier, Y.; Silbey, R.; Brédas, J.-L. *Chem. Rev.* **2007**, *107*, 926–952.

(37) Cave, R. J.; Newton, M. D. *Chem. Phys. Lett.* **1996**, *249*, 15–19.

(38) Larsson, S. *J. Am. Chem. Soc.* **1981**, *103*, 4034–4040.

(39) Kawatsu, T.; Coropceanu, V.; Ye, A.; Brédas, J.-L. *J. Chem. Phys. C* **2008**, *112*, 3429–3433.

(40) Mančal, T.; Valkunas, L.; Fleming, G. R. *Chem. Phys. Lett.* **2006**, *432*, 301–305.

(41) Newton, M. D. *Chem. Rev.* **1991**, *91*, 767–792.

(42) Prytkova, T. R.; Kurnikov, I. V.; Beratan, D. N. *J. Phys. Chem B.* **2005**, *109*, 1618–1625.

(43) Van Voorhis, T.; Kowalczyk, T.; Kaduk, B.; Wang, L. P.; Cheng, C. L.; Wu, Q. *Ann. Rev. Phys. Chem.* **2010**, *61*, 149–170.

(44) Kong, J. et al. *J. Comp. Chem.* **2000**, *21*, 1532–1548.

(45) Becke, A. D. *J. Chem. Phys.* **1988**, *88*, 2547.

(46) Peumans, P.; Bulović, V.; Forrest, S. R. *Appl. Phys. Lett.* **2000**, *76*, 2650–2652.

(47) Kim, I.; Haverinen, H. M.; Wang, Z.; Madakuni, S.; Kim, Y.; Li, J.; Jabbour, G. E. *Chem. Mater.* **2009**, *21*, 4256–4260.

(48) Triyana, K.; Yasuda, T.; Katsuhiko, F.; Tsutsui, T. *Thin Solid Films* **2005**, *477*, 198–202.

(49) Schaafsma, T. J. *Sol. Ener. Mat. Sol. Cells* **1995**, *38*, 349–351.

(50) Vilmercati, P. et al. *Surface Science* **2006**, *600*, 4018–4023, Berlin, Germany: 4-9 September 2005, Proceedings of the 23th European Conference on Surface Science.

(51) Scandola, F.; Chiorboli, C.; Prodi, A.; Iengo, E.; Alessio, E. *Coord. Chem. Rev.* **2006**, *250*, 1471–1496.

(52) Fischer, H.; Wenderoth, H. *Annalen* **1940**, *545*, 140–147.

(53) Woodward, R. B. et al. *J. Am. Chem. Soc.* **1960**, *82*, 3800–3802.

(54) Difley, S.; Wang, L.-P.; Yeganeh, S.; Yost, S. R.; Van Voorhis, T. *Accounts of Chemical Research* **2010**, *43*, 995–1004.

(55) Aaqvist, J.; Warshel, A. *Chem. Rev.* **1993**, *93*, 2523–2544.

(56) Cramer, C. J.; Truhlar, D. G. *Chem. Rev.* **1999**, *99*, 2161–2200.